

RECENT DEVELOPMENTS IN EDDY CURRENT TESTING

Gerd Dobmann, Kurt Betzold, and Paul Höller

Fraunhofer-Institut für zerstörungsfreie Prüfverfahren
D-6600 Saarbrücken 11
Federal Republic of Germany

INTRODUCTION

From the point of material fatigue and corrosion the objective and quantitative inspection of surfaces and near-surface zones in metallic components by NDT methods are of interest. Eddy-current methods in particular are suitable to solve this inspection problem. In the last years the electric current perturbation was investigated with the special case of yoke magnetization and signal pick-up by magnetic tapes. Finite element codes were applied to bring better interpretation in eddy-current testing, i.e. for the modeling of special interpretation problems in steam generator tube inspection.

MAGNETIC PICK-UP OF EDDY-CURRENT IMAGES

The fact that electric current lines are disturbed by defects, i.e. by surface-breaking cracks, has been well-known for many decades. With d.c. [1] and a.c. [2] potential drop arrangements the detection of cracks and the measurement of the crack-height has been investigated and developed. The disadvantage is the need of electrical contact for an electric voltage or resistivity measurement. The proposal to measure the magnetic fields of the disturbed current lines instead of the electric voltage by using small noncontacting Hall-element probes is traced back to F. Förster [3] for d.c. application. Since 1969 [4] the electric-current perturbation method has been further developed. The electric current is introduced by ohmic contacts or as eddy currents produced by the induction field of a magnetic pick-up coil; frequencies less than 100 Hz to 100 kHz are used depending on the depth of the defect to be detected (surface and sub-surface defects) and the conductivity of the nonferromagnetic materials [5,6]. For the magnetic field measurement special Hall-element probes to measure the tangential component in a differential arrangement are developed. For the low-frequency range (depth of current penetration \gg defect depth) a semi-analytical two-dimensional approach is available, basing on conformal mapping and Biot-Savart law. With this model an excellent qualitative agreement between theory and experiment is obtained. The technique is not only a sensitive

method for flaw detection (crack length < 0.45 mm) but also offers better interpretation by the analysis of signal shapes and amplitudes.

The inspection problem to detect and localize small cracks in ferritic welds with high permeability gradients (not stress relieved welds in the steel-globe of a PWR-containment) was solved by magnetographic inspection [7]. During magnetization with a 50 Hz handyokey (Fig. 1) the demagnetized tape is pressed on the surface to be inspected. The leakage field tangential components of the defect are stored in the tape after switching off the magnetization. The tape is analyzed in a special equipment, where a tape-recorder head as an induction coil probe fixed on a rotating disk (50 Hz rotating frequency, d.c. motor drive) scans the tape. The stored leakage fields of defects induce an electric voltage which is modulated by the scan frequency signal. The resulting signal and a trigger signal are transmitted by a cylindrical pot magnet transformer from the rotating part in the fixed part of the equipment (frequency range ≤ 50 kHz). After the separation of the 50 Hz rotating frequency signal (fixed high pass filter) the signals are evaluated with variable filters and indicated in an A-scan on a CRT-display. Figure 2 gives an example for the detection of an EDM-notch (length 2 mm, width 26 μm , height 30 μm) in a ferritic weld. Before filtering, the defect signal is superimposed by spurious indications of the multilayer submerged-arc weld. After filtering, the signal-to-noise ratio is enhanced on 9 dB.

Additionally to the experimental investigations, a numerical integral-equation approach for the calculation of magnetic leakage fields of defects and a.c. magnetization was developed [8].

Stimulated by the SwRI results with current-perturbation-probe scanning and the high sensitivity of the magnetographic inspection in the case of defects in ferritic materials in the IzfP, investigations are initiated for the application on nonferromagnetic materials, i.e. austenitic steels, welds and claddings.

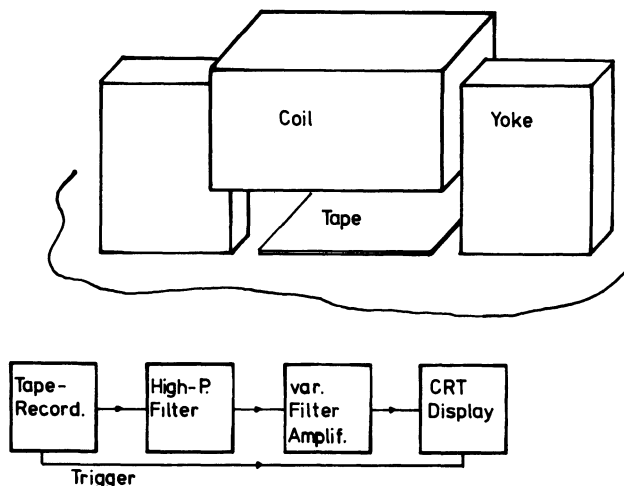


Fig. 1. Magnetic pick-up by tape

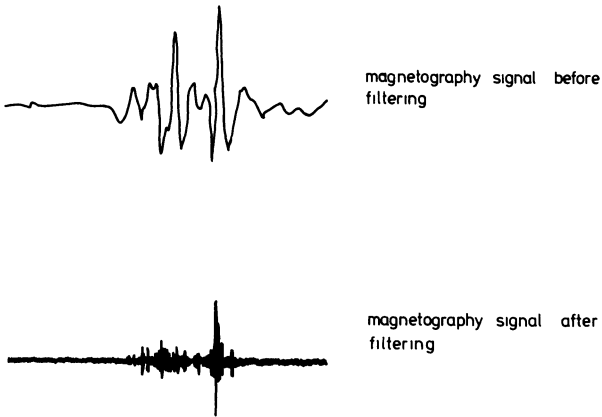


Fig. 2. Slit-length 2mm, width 26 μm , height 30 μm

In ferritic steels the largest defect/magnetic field interaction is obtained for a magnetization direction perpendicular to the crack direction (magnetic leakage flux). Nevertheless, a magnetic field flow parallel to a crack (eddy current flow perpendicular to the crack) yields two crack-tip current perturbation signals from both ends of the crack, which are only a little smaller than the leakage flux signals.

Figure 3 shows an example for an artificial defect (saw-cut, length 20 mm, width 0.1 mm, height 1 mm) in a ferritic steel and an austenitic

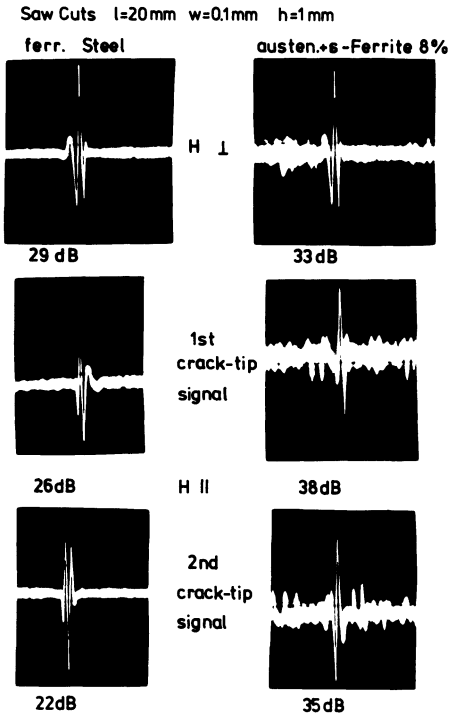


Fig. 3. Magnetic tape filtered signal, 50 Hz yoke-magnetization

steel with 8 % δ -ferrite content. The magnetic field was produced in a 50 Hz hand-yoke with an amplitude of 150 A/cm. The defect signals are stored in a commercial magnetic tape, evaluated by high-pass filtering on the tape-recorder equipment previously described. The A-scans on the CRT-display are amplified on the same amplitude level, the amplification in dB is indicated. In all cases the scan direction is perpendicular to the crack-lengthwise direction.

For magnetic field flow perpendicular to the crack the defect signal in the austenitic steel asks for 4 dB higher amplification than the same defect in the ferritic steel. In the other case (magnetic field flow parallel to the crack) the current perturbation signals in austenitic steel need 13 dB more amplification to produce the same amplitude level as the signals in the ferritic steel. Because of this higher amplification the noise in the signals obtained on austenitic steel is much higher than in the ferritic case, furthermore, on austenitic steel leakage fields produced by the exciting coil of the yoke and the yoke geometry have more influence on the tape inhomogeneities.

Figure 4 shows the application of the magnetic field flow perpendicular to the lengthwise direction of an artificial defect (saw-cut, height 3 mm, length 12 mm, width 0.5 mm) in nonferrous material, i.e. a copper sheet of 5 mm wall-thickness. The recorded magnetic tape signals with scan paths perpendicular to the defect are indicated along the defect length. In the image plane a maximum of the leakage field amplitude occurs for $y = 1/2$, the signal shape (north-south-pole characteristic) does not change the sign along the length.

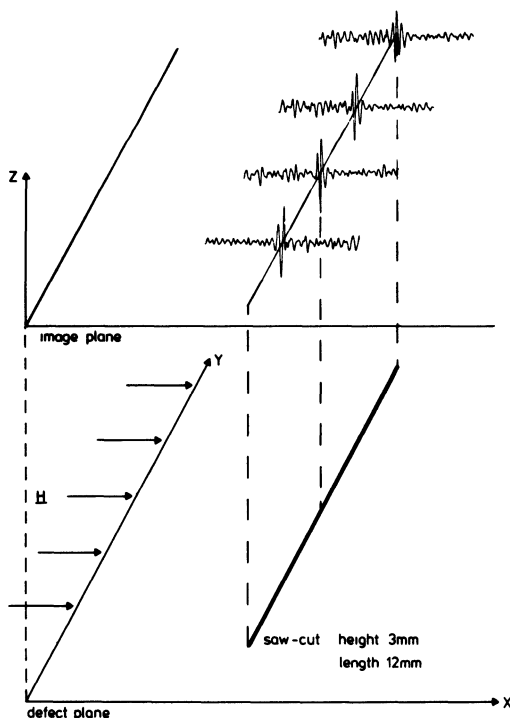


Fig. 4. Specimen-Cu-sheet, 5 mm wall-thickness, magnetizing fieldstrength $H = 150$ A/cm, perpendicular to the defect $H \perp$

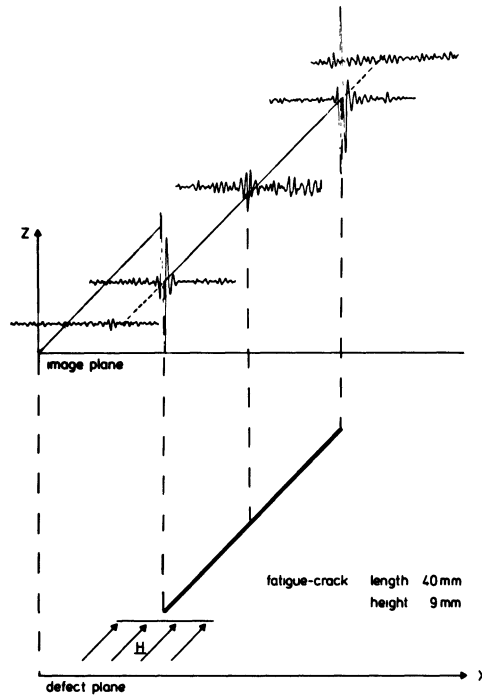


Fig. 5. Specimen austenitic steel sheet, 20 mm wall thickness, magnetizing fieldstrength $H = 150$ A/cm parallel to the defect $H \parallel$

Figure 5 shows an example for the leakage field image for the magnetic field flow parallel to the length of an artificial defect (saw-cut, length 40 mm, height 9 mm, width 0.5 mm) in an austenitic steel sheet of 20 mm wall-thickness. Similar to the electric current perturbation results of SwRI [6] two amplitude maxima with opposite sign occur near the defect ends. The field intensity in Figs. 4, 5 with 150 A/cm was the same.

The integral equation software to calculate magnetic leakage fields of rectangular artificial defects of finite length, width and height (3D-approach) was adapted to austenitic steels, higher frequencies and the case of magnetic field flow parallel to the defect length. Nevertheless the software development is not complete, because the influence of induced surface-current-densities on the two smaller crack flank surfaces (along the defect width) is neglected. Figures 6, 7 and 8 show the rectified amplitude-locus curves of calculated ECP-defect signals for different crack length (length 2, 1.6, 0.8 mm, width 0.2 mm, height 0.8 mm). In the upper part the tangential component of the stray-field H_x (x - direction perpendicular to the magnetic field flow, parallel to the eddy current flow) and in the lower part the normal component H_z are indicated. The peak-to-peak distance in H_z gives a linear correlation to the defect length, the peak-amplitudes are a complex function of the defect length, width and height and have been further investigated.

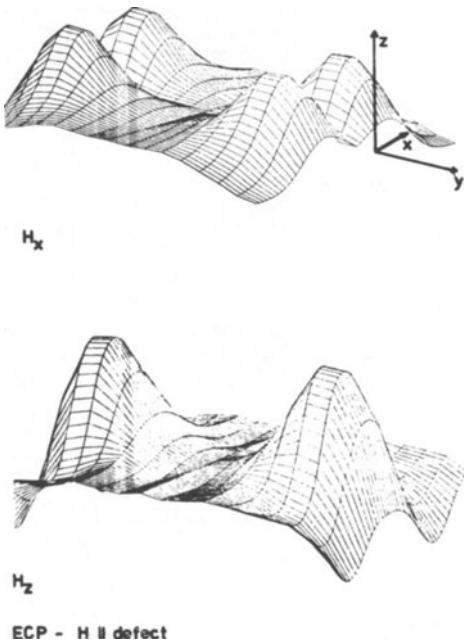


Fig. 6. Crack length 2 mm, width 0.2, height 0.8 mm

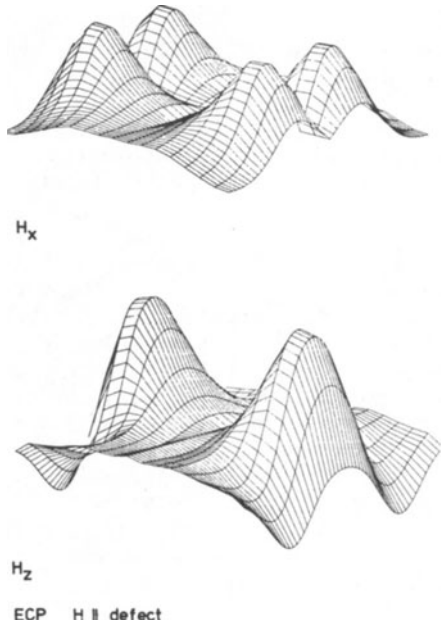


Fig. 7. Crack length 1.6 mm, width 0.2, height 0.8 mm

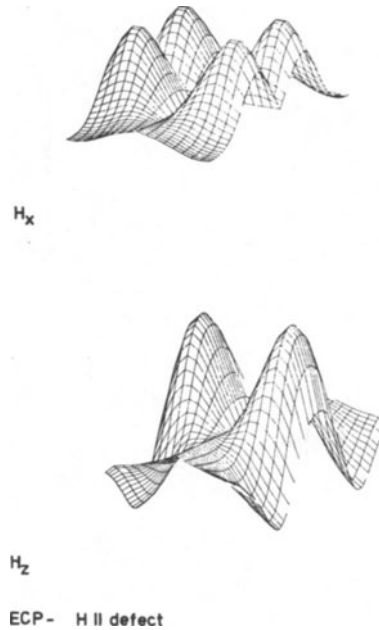


Fig. 8. Crack length 0.8 mm, width 0.2, height 0.8 mm

The figures 9, 10, 11 show the rectified amplitude-locus curves of calculated ECP-defect signals for the same crack-length of 2 mm, but different widths (0.15, 0.2, 0.25 mm) and heights (0.6, 0.8, 1.0 mm) and the magnetic field flow perpendicular to the lengthwise direction of the defect. The influence of the increasing defect volume is indicated by an increase in peak amplitude and peak separation in crack-width direction. Undoubtedly, the defect signal amplitudes increase with the eddy current density, this means with an increase of the magnetic field amplitude. This fact is important especially for the detection of subsurface defects. Figure 12 shows examples of two different artificial surface defects (saw-cuts, length 26 mm, width 0.1 mm, height 2 and 4 mm) in an austenitic steel sheet of 6 mm thickness. For an inspection from the defect-free surface the defects on the opposite surface act like subsurface defects with depths of 2 mm and 4 mm below the surface. For a magnetic field flow parallel to the crack lengthwise direction, only one of the two ECP-signals is evaluated, the magnetizing frequency was 50 Hz sinusoidal with a field amplitude of 1000 A/cm. From the signal-to-noise ratio we can see that the detectability decreases roughly with the defect depth below the surface. The S/N is 20 dB for the defect with 2 mm depth below the surface (height 4 mm) and decreases to 7.7 dB for the defect with 4 mm depth below the surface (height 2 mm), near the 6 dB-limit of detectability.

Further investigations are related to the use of pulse magnetization, the optimization of the shape of the current pulse and the magnetization facilities like air-coils and electromagnetic yokes.

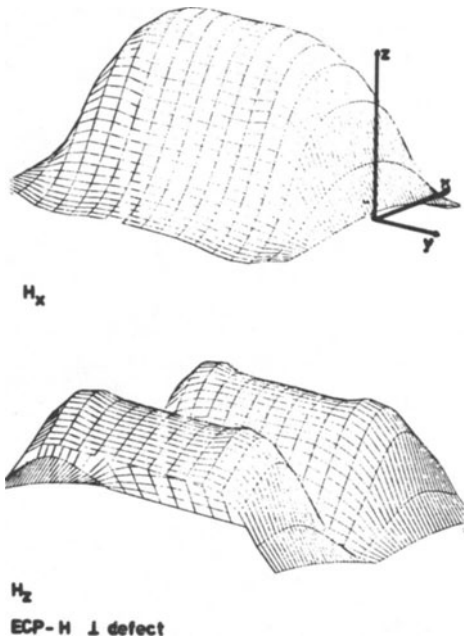


Fig. 9. Crack length 2mm, width 0.25, height 1 mm

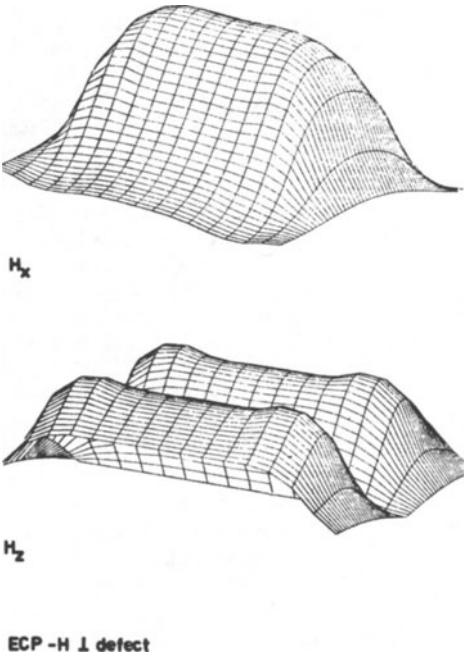


Fig. 10. Crack length 2 mm, width 0.2, height 0.8 mm

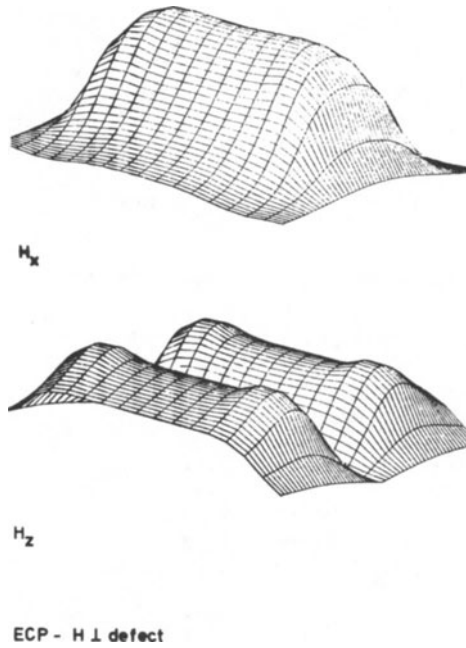


Fig. 11. Crack length 2 mm, width 0.15, height 0.6 mm

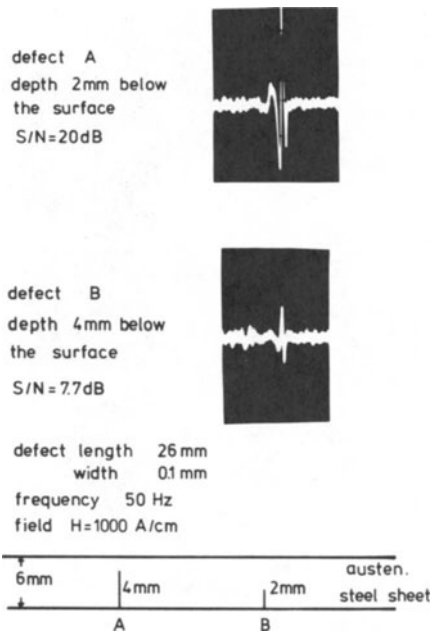


Fig. 12. ECP-Tapesignals of subsurface defects

Figure 13 shows an example of pulse magnetization with an electromagnetic yoke. The pulse amplitude was 1.6 kA, the rise-time was 2 ms, the fall-time 4 ms. The ECP-signals of three defects (EDM-notches) are indicated after high-pass filtering of the tape for the same amplification. The upper part presents the signal of a notch with length 10 mm, width 0.16 mm, height 1.55 mm, in the middle part the notch has a length of 8 mm, a width of 0.14 mm, a height of 1.05 mm, the lower part indicates the notch signal with a length of 5 mm, a width of 0.14 mm, and a height of 0.51 mm. The signal-to-noise ratio is 17 dB, 12 dB and 7 dB, respectively. The thickness of the austenitic steel sheet is 25 mm.

FINITE ELEMENT MODELING OF EDDY-CURRENT TESTING

Numerous computations have been performed and verified against experiments at IzfP in Saarbrücken (9, 10). The main objective for the practical use of the code was to produce signal loci as they occur during the inspection. By systematic variation of the input parameters a catalogue of signal loci can be produced in order to support the interpretation of the measured signals. The following examples can demonstrate this ability.

Figure 14 shows eddy current signals from a coaxial inner coil in absolute arrangement in a steam generator tube when passing the upper edge of the tube sheet and the rolling region; the distance between these both influences has been varied between 1 and 9 mm according to variations during fabrication. The signals on the left hand side are computed predictions; the encircled part of the signals has been experimentally verified, the working point of the coil in the normalized impedance plane for 100 kHz in the free region of the tube is outlined in the lowest picture (1). The dotted line indicates the impedance curve for various frequencies. When moving the coil towards the edge of the

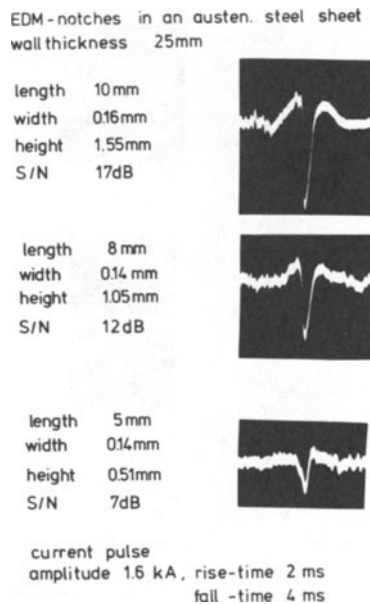


Fig. 13. ECP-Tapesignals of surface defects, pulsed yoke magnet.

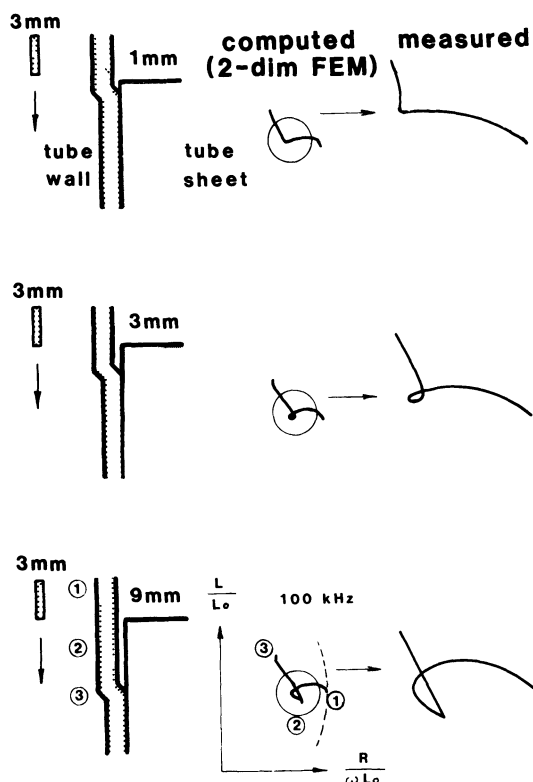


Fig. 14. Eddy current signals of coaxial inner coils in the tube sheet region

tube sheet, the signal follows the curve until (2), stays there for a while, and finally it reaches (3) when the coil comes to the rolling region. The smaller the distance between the edge of the tube sheet and the rolling the more the coil integrates over the corresponding signals. In order to check the quality of the computed signals the same configuration has been fabricated and inspected. The measured signals are shown on the right hand side; they correspond to the encircled part of the computed signals.

The next step was to investigate the influence of various deposit materials. Figure 15 shows a comparison between measured and computed signals for magnetic sludge around the tube. At this point it is obvious that a measurement of the electrical and magnetical properties of the magnetite must be performed in advance in order to provide typical input data for the code. The right hand side shows measured signals for different concentrations. The phase angle is not dependent on the concentration. The cross of dotted lines indicates the working point of the coil in the free region of the tube. Computed results for incremental permeabilities of 5 and 10 are shown on the left hand side.

In order to tackle the problem of copper deposit two different models are used. The first one puts a solid sheet of copper around the tube. According to the finite element discretisation of the region three different sheets of 0.04 mm (1 element), 0.08 mm (2 elements) and 0.25

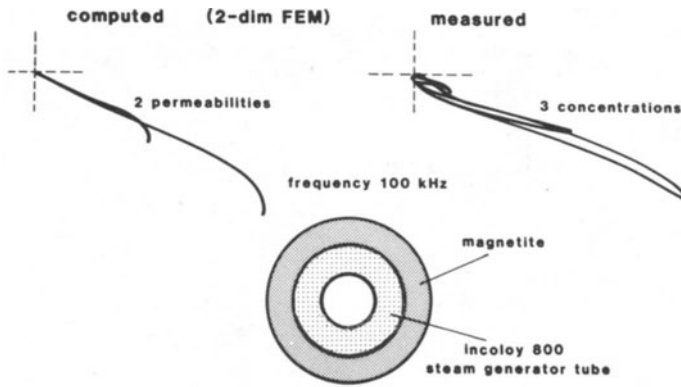


Fig. 15. Eddy current signals of coaxial inner coils for magnetite deposit

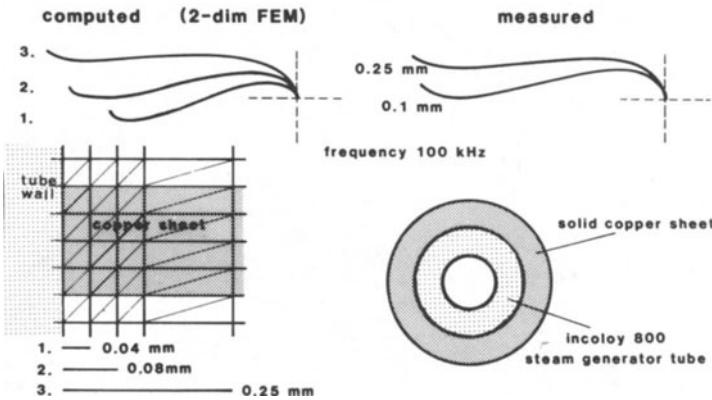


Fig. 16. Eddy current signals of coaxial inner coils for a solid copper sheet

mm (4 elements) have been considered. The corresponding loci curves are shown on the left hand side of Fig. 16. The agreement with two measured signals shown on the right side is fairly good. In the experiment we used two thin solid copper sheets which we put very close around the tube.

A second model uses copper sludge made from a mixture of copper dust and chips and water. When the coil was moved along this sludge, there was no resulting signal with the gain level of Fig. 16. After having increased the gain level, the small egg-shaped signal on the right side of Fig. 17 was detected; as reference the signal of a hole through the wall with a diameter of 1 mm is drawn. When trying to repeat the experiment two days later, the signal had turned the phase angle and reduced its amplitude because the copper parts have been corroded on the surface. With respect to modeling this sludge with a finite element code, a rough approach can be to describe the metal chips with three-dimensional elements of copper with contact at the edges. The axisymmetric 2-dim discretisation uses circumferential elements, representing closed

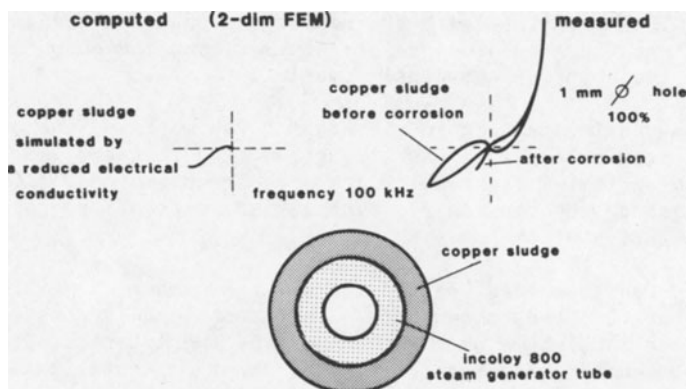


Fig. 17. Eddy current signals of coaxial inner coils for copper deposits

loops for the eddy currents. To use the 2-d code nevertheless, a very crude approach was made which neglects the physics of the problem and simply reduces the electrical conductivity in the sludge region. The resulting computed signal is shown on the left hand side. This approach is very similar to the one of Steve Brown (EPRI-NDE Center) for simulation of IGA in Inconel tubing.

The next step was to apply the FE-code for a copper sheet in the crevice gap between tube and tube sheet. The computed result is shown on the left side of Fig. 18; the cross characterizes once more the working point for the coil in the free region of the tube (1) whereas the end point (3) corresponds to the coil in the rolling region of the

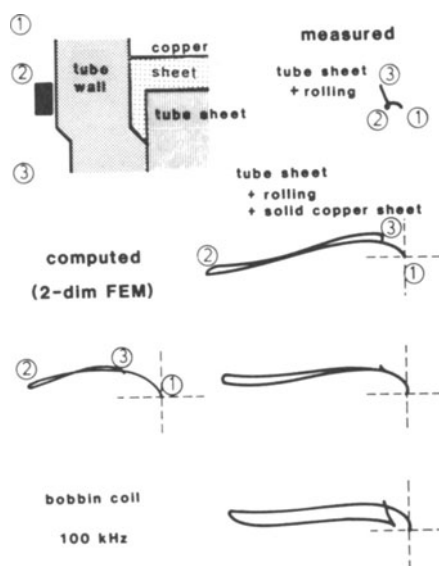


Fig. 18. Eddy current signals of coaxial inner coils for copper sheet in the crevice gap region

tube sheet. The comparison with the measured signals on the right hand side shows that the signal shapes are similar, but the computed loop produced by the copper is obviously smaller.

For a magnetite deposit in the crevice gap we found the opposite effect; the predicted signal was stronger varied than the experimental set up could verify. These results are not yet understood. Actually we are checking both the experiment which is very delicate to perform and the discretisation of the code.

The 2-d-code has been applied for a large number of problems - some of them have been shown here - and it could be demonstrated that the code is an invaluable help for supporting the interpretation of signals produced by axisymmetric effects. For the special example of the rolling of the tube in the tube sheet (Fig. 14) it has been outlined that even the smallest details can be predicted; but the limits are getting obvious when looking at the signals produced by deposits in the crevice gap region (Fig. 18).

REFERENCES

1. B. M. Thornton and W. M. Thornton, The detection of cracks in castings by an electrical method, Foundry Trade Journal 65:253 (1941)
2. A. Troost, Ermittlung von Rissen und Messung der Rißtiefen in metallischen Werkstoffen durch elektrische Spannungsmessung, Metallwirtschaft 23 (1944)
3. R. C. McMaster, Nondestructive Testing Handbook, Vol. II, Ronald Press Company, New York (1963), p. 34.21
4. F. N. Kusenberger, P. H. Francis, B. E. Leonard, and J. R. Barton, Nondestructive Evaluation of Metal Fatigue, AFOSR 69-1429TR (1969)
5. R. E. Beissner, C. M. Teller, G. L. Burkhardt, R. T. Smith, and J. R. Barton, Detection and Analysis of Electric-Current Perturbation Caused by Defects, ASTM STP 722 (1981)
6. C. M. Teller and G. L. Burkhardt, Small defect characterization by the electric current perturbation method, in: "Proceedings of the 13th Symposium on NDE," San Antonio, Tx (1981)
7. G. Dobmann, H. Persch, G. Walle, and U. Coehne, Objective magnetic leakage flux testing for the interpretation of magnetic particle pseudo-crack indications in nuclear power plants, in: "Proceedings of the 4th International Conference on NDE in Nuclear Industry," Deutsche Gesellschaft für Zerstörungsfreie Prüfung, Berlin (1981)
8. G. Walle and G. Dobmann, A model for the interpretation of a.c. magnetic stray flux measurements, in: "New Procedures in NDT," P. Höller, ed., Springer-Verlag, Berlin, Heidelberg, New York, Tokyo (1983)
9. R. Palanisamy, Finite element modeling of eddy current nondestructive testing phenomena, Dissertation, Colorado State University, Fort Collins, Colorado (1980)
10. N. Ida, K. Betzold, and W. Lord, Finite element modeling of absolute eddy current probe signals, Journal of NDE 3(3):147(1982)